PHYSICAL REVIEW B VOLUME 50, NUMBER 5 1 AUGUST 1994-I

Temperature dependence of resonant x-ray magnetic scattering in holmium

G. Helgesen,* J. P. Hill, T. R. Thurston, and Doon Gibbs
Department of Physics, Brookhaven National Laboratory, Upton, New York 11973

J. Kwo and M. Hong
AT&T Bell Laboratories, Murray Hill, New Jersey 07974

(Received 28 February 1994)

We report the results of resonant x-ray magnetic scattering experiments on bulk and thin-film single crystals of holmium. The scattering at the principal magnetic reflection has been characterized as a function of the temperature in the spiral phases near and below their respective Néel temperatures. The integrated intensity of the principal magnetic peak in both samples shows power-law behavior versus reduced temperature with nearly equal exponents. The exponents for the scattering at the resonant second and third harmonics in the bulk sample are not simple integer multiples of the first, and motivate the consideration of simple scaling corrections to mean-field theory. We also present and compare the results of high-resolution measurements of the temperature dependence of the magnetic wave vectors, c-axis lattice constants, and correlation lengths of the magnetic scattering of the two samples in their spiral phases. Although the qualitative behavior is similar, systematic differences are found, including uniformly larger magnetic wave vectors and the suppression of the 1/6 phase in the film. The spiral magnetic structure of the film forms a domain state at all temperatures in the ordered phase. The magnetic correlation lengths of both samples are greatest near the Néel temperature, where that of the film appears to exceed the translational correlation lengths of the lattice. As the temperature decreases, the magnetic correlation lengths also decrease. These results are discussed in terms of the strain present in the samples.

I. INTRODUCTION

Neutron-diffraction studies of the long range magnetic order in the rare-earth metals began in the 1950's, and were especially stimulated by the growth of the first high-purity single crystals in the 1960s. Since that time, there has been extensive experimental and theoretical work utilizing a wide range of techniques, and a basic understanding of rare-earth magnetism is now well established.[1] One interesting, recent direction for research in characterizing the magnetic and structural properties of rare earths has involved the application of high-resolution x-ray-scattering techniques, particularly through the use of high brightness beams from synchrotron sources.[2] In addition, the growth of thin films and superlattices by molecular beam epitaxy (MBE) techniques has introduced a new regime of rare-earth magnetism which increasingly illustrates the delicate balance of elastic and magnetic interactions in the ordered phases, and has opened the possibility of tailoring the magnetic properties.[3-7]

In order to shed light on the origin of the complex low-temperature phase behavior, we have carried out a series of resonant x-ray magnetic scattering studies of bulk and thin-film single crystals of holmium. For these experiments the principal difference between the two samples lies in the manner in which the probed volume is strained by its environment. In the case of the film, the lattice mismatch with the substrate causes a tensile in-plane stress, and a corresponding contraction along the c axis. For the bulk sample, there are strains associated with the surface preparation process, specifically involving chemical and structural defects, which may influence the magnetic structure within typical x-ray penetration depths (≈ 1 μm for rare earths). For both the bulk and thin-film samples, there are additional strains associated with magnetoelastic coupling, which arise below the Néel temperature T_N in the magnetically ordered phase. It should be noted that elucidating the role of strain in determining interface and thin-film magnetic structure, and the dependence of the latter on substrate mismatch and film thickness are current areas of active research.[3-7] In this regard, the separate effects of interfacial clamping and magnetoelastic strain on the ferromagnetic transition of various Dy multilayers and films have recently been discussed in papers by Beach *et al.*[4] and Tsui and Flynn.[5] Related problems in Ho films and multilayers have been studied by neutron scattering by Jehan *et al.*[6] and Swaddling *et al.*[7]

The magnetic structure of bulk holmium in its magnetically ordered phase has been extensively characterized in a number of x-ray- and neutron-scattering experiments.[8-15] The main effects are determined by the competition among the indirect exchange, crystal-field, and magnetoelastic contributions to the free energy.[1] The critical properties, however, of holmium (and, indeed, of all the rare earths) have remained controversial. Assuming that the magnetic ordering transition is second order, various experimental determinations of the critical exponent of the order parameter, β, and of the exponent of the specific heat, α, have been found to disagree.[16] On the basis of dilatometry measurements, it has been sug-

0163-1829/94/50(5)/2990(15)/$06.00

gested that the magnetic ordering transition may be discontinuous,[17] and neutron-scattering studies of holmium have reported hysteresis in the intensity dependence of the magnetic scattering near T_N.[18] On the theoretical side, there are at least two proposed universality classes for the rare-earth magnetic spirals, including a symmetric $O(n)$ model with $n=4$ (Ref. 19) and the chiral universality class.[20] In contrast, Barak and Walker[21] have proposed that the transformation is driven first order by fluctuations and Azaria *et al.*[22] have suggested that the critical behavior is controlled by tricritical points in the phase diagram.

Very recently, in high-resolution x-ray- and neutron-scattering experiments, Thurston *et al.*[23] demonstrated the existence of two components in the critical magnetic fluctuations of holmium above T_N, instead of one, as would be expected in an ideal system. Two-component line shapes in the critical scattering have since been found in various other rare earths and actinides, including Tb, NpAs, and UO_2.[24–26] They have also been seen earlier in the critical fluctuations of several perovskites near their cubic-to-tetragonal structural phase transformations.[27,28] A variety of different measurements have suggested that the longer-ranged fluctuations may be associated with the strain localized at or near the surface. While detailed theoretical models are lacking, the second length scale observed in the perovskites has also been attributed to the influence of a random distribution of defects at a first-order phase transition.[27,28]

In this paper, we characterize the temperature dependence of the magnetic scattering at the principal magnetic satellite and at two higher harmonics in the ordered phase near and below T_N. The integrated intensity of the principal magnetic scattering in both bulk and film samples shows power-law behavior versus reduced temperature, with nearly equal exponents. The exponents found for the higher harmonics of the bulk sample are not integer multiples of the exponent for the principal satellite. Therefore, we also discuss possible scaling corrections to mean-field behavior. Interestingly, we find that a one-parameter correction to mean-field scaling, originally developed for the three-dimensional (3D) *XY* model,[29,30] is sufficient to collapse the intensities of the principal and higher harmonics onto a universal curve. Hopefully, these results will stimulate renewed consideration of the universality class appropriate for the spiral rare earths. Related studies have been reported for the first and second harmonic critical behavior of charge-density waves in liquid crystal systems by Wu *et al.*[31] We also present and compare high-resolution measurements of the temperature dependence of the magnetic wave vectors, *c*-axis lattice constants, and correlation lengths of the magnetic scattering in the bulk and thin-film samples. Although the qualitative behavior is similar, systematic differences are found, including uniformly larger magnetic wave vectors and the suppression of the $\frac{1}{6}$ phase in the film. These results are somewhat surprising in view of the expectation that bulk properties might be recovered in a 2 μm thick film. They are reminiscent of earlier studies of Dy and Ho thin films and multilayers,[3–7] and are discussed in terms of the differing strains in the two samples. We have also found that the spiral phase of the thin film forms a domain state at all temperatures below T_N. Remarkably, the magnetic correlation lengths of both samples are greatest near T_N, and that of the film exceeds the translational correlation lengths of the lattice.

Before turning to the presentation of our results, we note several reasons why it is interesting to reinvestigate the magnetic properties of rare-earth, actinide, and transition element antiferromagnets by x-ray-scattering techniques. First, the x-ray resolution is typically a factor of 10 narrower than that employed in neutron-scattering experiments. Thus, assuming that x-ray magnetic scattering is observable, it is possible to probe correlation lengths an order of magnitude greater than with neutrons. Second, the relative weakness of the x-ray magnetic cross section offers the advantage of extinction-free determinations of critical exponents below T_N. Third, the existence of resonant higher harmonics, associated with the electric dipole and quadrupole contributions to the cross section, has opened up the possibility of testing scaling predictions in incommensurate antiferromagnets. An interesting variation of this has already been studied in the scattering associated with lattice modulations in thulium.[32] Fourth, in all studies of critical behavior, the broad energy resolution characteristic of most x-ray-scattering experiments (5–10 eV) insures that the quasielastic approximation is exact, simplifying the analysis. Finally, as a result of the variable penetration depth, x-ray scattering is especially sensitive to surface and "near-surface" (0–10 μm) magnetic properties.

This paper is organized as follows. In Sec. II, we briefly describe the magnetic structure of holmium. Section III presents the elements of the x-ray resonant magnetic cross section which are relevant to the present work. The details of the experiments are presented in Sec. IV. Our main results and discussion are given in Sec. V, and our conclusions in Sec. VI.

II. MAGNETIC STRUCTURE OF HOLMIUM

The hcp metal holmium has 10 $4f$ electrons in a $^5I_8$ ground state with 3 electrons in the $5d$ and $6s$-$6p$ conduction bands.[1] Below the Néel temperature $T_N \approx 131$ K, the magnetic moments in Ho ($\approx 10\mu_B$ per atom) are oriented perpendicular to the crystalline *c* axis, which reflects the dominant term of the crystal field in the free energy. Within the crystalline *a*-*b* plane the spins are ferromagnetically ordered. However, the spatial direction of the moments rotates from basal plane to plane creating a spiral structure propagating along the *c* axis. The average rotation of the moments per plane may be characterized by the phase angle $\varphi = \tau\pi$, where τ is the wave vector of the magnetic modulation. Close to T_N, $\tau \approx 0.28$, and decreases with decreasing temperature. At $T_C \approx 20$ K, bulk Ho has a first-order phase transition to a conical magnetic phase with a ferromagnetically ordered component of the magnetic moment along the *c* axis in addition to the planar spiral component.

Neutron-scattering experiments have shown that between 10 and 80 K, there are additional fifth- and seventh-order harmonics along the $(0,0,L)$ direction.[1,3,6–9,15] These occur because of the tendency of the sixfold crystalline anisotropy to align the moments along the six easy axes within the basal planes. At low temperatures, in the conical phase, the average magnetic phase angle between spins on two neighboring planes equals 30°, but the structure consists of "bunched" doublets of spins oriented along the six easy axes. The magnetic structures which occur above T_C can be described using combinations of doublets and spin discommensurations, or spin slips, in which only one atomic plane has moments associated with a particular easy direction.[11,12] Commensurate spin-slip structures correspond to those with rational ratios between numbers of doublets and spin slips. Incommensurate and disordered spin-slip structures may also be defined and are discussed in more detail in Appendix B. Refinements of this simple spin-slip picture on the basis of extensive neutron-scattering and ultrasound experiments have been suggested by Cowley and Bates.[15,33] None of the models proposed for the magnetic structure of holmium has predicted the existence of even order magnetic structural harmonics along the c axis and none has been observed.

III. RESONANT X-RAY MAGNETIC SCATTERING

The scattering of x rays by ordered magnetic moments was first demonstrated in NiO by de Bergevin and Brunel,[34] and later in Ni (Ref. 35) and rare-earth metals.[2,11–14,32] Although x-ray magnetic scattering from holmium can be detected over a wide range of x-ray energies, there is a 50-fold resonant enhancement of the magnetic scattering, when the incident photon energy is tuned to the $L_{\rm III}$ absorption edge.[13,14] Similar and even larger resonant enhancements have been observed at the M edges of actinide compounds,[36,37] while the transition elements Ni and Fe show enhancements at the L edges.[38,39]

Earlier resonant studies of holmium have shown that near the $L_{\rm III}$ absorption edge ($E=8067$ eV) there are maxima in the energy dependence of the principal magnetic scattering at two different incident photon energies.[13,14] At $E=8072$ eV there is an electric dipole ($E1$) transition from the $2p_{3/2}$ orbital to the $5d$ band, and at $E=8064$ eV there is an electric quadrupole ($E2$) transition from the $2p_{3/2}$ to the $4f$ orbitals. The theory for resonant magnetic scattering has been worked out by Hannon *et al.*[40] and a detailed calculation for the magnitude of the resonant scattering in different rare-earth metals has been given by Hamrick.[41] The magnetic scattering amplitude for the electric dipole transition is given by[40]

$$f_{E1}^{\rm res}=\frac{3}{4}\frac{\lambda}{2\pi}\{(\mathbf{e}_i\cdot\mathbf{e}_f^*)A_0+i(\mathbf{e}_i\times\mathbf{e}_f^*)\cdot\hat{\mathbf{z}}A_1+(\mathbf{e}_i\cdot\hat{\mathbf{z}})(\mathbf{e}_f^*\cdot\hat{\mathbf{z}})A_2\}\ . \tag{1}$$

$\mathbf{e}_i$ and $\mathbf{e}_f$ are the polarization vectors of the incident and the scattered photons, $\hat{\mathbf{z}}$ is a unit vector in the direction of the magnetic moment, $A_0=F_{11}+F_{1\text{-}1}$, $A_1=F_{11}-F_{1\text{-}1}$, and $A_2=2F_{10}-F_{11}-F_{1\text{-}1}$, where

$$F_{LM}=\sum_{a,b}\frac{p_a p_{a(b)}\Gamma'(aMb;EL)}{2[E_b-E_a-E]-i\Gamma(b)}\ . \tag{2}$$

Here p_a and $p_{a(b)}$ are the probabilities that the ground state $|a\rangle$ with energy E_a is occupied and that the excited state $|b\rangle$ with energy E_b is empty, respectively. E is the energy of the incident photon. $\Gamma'(aMb;EL)$ is the partial width of the EL transition from $|a\rangle$ to $|b\rangle$ and $\Gamma(b)$ is the total width of the excited state $|b\rangle$(≈ 4.3 eV at the $L_{\rm III}$ edge in Ho). Since Γ' is proportional to the square of the overlap integral between the core electron and the excited valence electron, the resonance effect is strongest at the M edges ($3d\rightarrow 4f$) in the actinides and somewhat weaker at the L edges ($2p\rightarrow 4f, 2p\rightarrow 5d$) in the rare earths. The sensitivity to the magnetic ordering at the $E2$ transition occurs because the excitation involves an electronic transition to the partially filled and magnetically ordered $4f$ shell. For the dipolar $E1$ transition to the $5d$ band, the magnetic sensitivity is caused in part by the exchange splitting ($\ll 1$ eV in Ho) of the $5d$ band induced by the magnetic moment of the $4f$ shell. Recently, Carra *et al.*[42] and Luo *et al.*[43] have rewritten Eqs. (1) and (2) as tensor operators of the atomic spin and orbital magnetization densities. Further, Blume[44] has given an elegant, general derivation of the resonant x-ray cross section using symmetry arguments.

The first term in $f_{E1}^{\rm res}$ is independent of the direction of the magnetic moment and gives scattering at the position of the chemical Bragg peak. The second term depends linearly on the direction of the magnetic moment. For a magnetic spiral structure with wave vector τc^* along the c axis, this gives scattering at positions shifted by $\Delta Q_1=(0,0,\pm\tau)$ relative to the (H,K,L) Bragg peaks ($c^*=2\pi/c$ and the lattice constant $c=5.62$ Å at 90 K). The third term, which is quadratic in the direction of the magnetic moment, gives scattering at positions shifted by $\Delta Q_2=(0,0,\pm 2\tau)$ relative to the Bragg peaks, in addition to scattering at the same position as the chemical Bragg peak. Similarly, the scattering amplitude $f_{E2}^{\rm res}$ for the electric quadrupole transition contains 13 distinct terms[40] and gives rise to magnetic scattering peaks at reciprocal-lattice positions shifted by $(0,0,\pm\tau)$, $(0,0,\pm 2\tau)$, $(0,0,\pm 3\tau)$, and $(0,0,\pm 4\tau)$ relative to the Bragg peaks. It is important to note that the higher-order resonant harmonics occur independently of any deviations of the magnetic structure from pure spiral ordering. This is different from the occurrence of higher order magnetic harmonics in nonresonant magnetic x-ray scattering and in neutron scattering, which do not exist without distortions of the spiral structure. In the case of resonant x-ray magnetic scattering from a distorted spiral, the resonant and structural harmonics will interfere and, in principle, this is observable by characterizing the scattering versus incident photon energy. The presence of higher-order resonant harmonics in the cross section offers a unique opportunity to test harmonic scaling predictions in spiral magnetic structures.

IV. THE EXPERIMENT

The x-ray scattering experiments were performed on the bending magnet beamline X22C and on the 30-pole wiggler beamline X25 at the National Synchrotron Light Source at Brookhaven National Laboratory. Double-crystal Ge(111) and Si(111) monochromators were used on X22C and X25, respectively. On both beamlines, the scattered beam was analyzed using the (111) reflection of Ge, leading to an energy resolution of about 5–10 eV. Incident and scattered photons were detected using NaI scintillation counters. The tightest resolution obtained in these experiments was measured at the $(0,0,2-\tau)$ reflection of the bulk sample. The resolution widths were 6.7×10^{-4}, 4.1×10^{-4}, and 1.4×10^{-2} Å^{-1} full width at half maximum (FWHM) in the longitudinal, transverse, and out-of-plane directions, respectively. Both Ho samples were mounted in closed-cycle He refrigerators with temperature stability of ≈ 0.01 K over several hours. The temperature was monitored using Si-diode thermometers.

Two series of experiments were performed on the bulk sample, one with the energy tuned to the maximum scattered intensity at the dipolar $E1$ transition, which occurs at $E=8072$ eV, and the other at the quadrupolar $E2$ transition at $E=8064$ eV. The magnetic satellite at $\mathbf{Q}=(0,0,2-\tau)$ was found to have the highest intensity of the principal harmonics and was studied as a function of temperature at both these energies. The second-order satellite, located at $\mathbf{Q}=(0,0,2-2\tau)$, was measured at the dipolar $(E1)$ transition. The third-order satellite at $(0,0,2-3\tau)$, which has a vanishing x-ray-scattering cross section at the $E1$ transition, was measured with the x-ray energy tuned to the quadrupole $(E2)$ transition. The x-ray penetration depth in Ho is about 0.5 μm at these energies.

The surface of the bulk holmium sample ($4\times4\times9$ mm^3) was parallel to the (001) crystalline planes to within about 0.2°. It was first mechanically polished and then electropolished in a passivating methanol-perchloric acid solution. Scanning ion fluorescence measurements revealed no unusual chemical impurities at the surface. Structural defects such as pits, with length scales on the order of microns, were evident in scanning electron measurements. The mean-square roughness as determined by x-ray reflectivity measurements in air was 20 Å, or greater. The mosaic of the bulk sample was less than 0.01° FWHM. Variable energy positron annihilation experiments indicate a high vacancy defect density ($\sim10^{18}$ cm^{-3}) within a few hundred angstroms of the surface of the bulk sample and a lower defect density ($\sim10^{16}$ cm^{-3}) extending to about 0.5 μm beneath.[45] More detailed information concerning the defect structure will require systematic studies of several samples with controlled defect densities.

In addition to the bulk sample, a thin Ho film was also studied. This sample is a sandwich consisting of a sapphire (Al_2O_3) substrate, a 2000-Å Nb(110) buffer layer, a 2400-Å Y(001) layer, a 2-μm-thick Ho(001) layer, and a 30-Å Y cap.[3] The mosaic of the Ho layer was about 0.11° FWHM. It seems likely that the larger mosaic in the film, as compared to the bulk, originates from the lattice mismatch (2%) of the Ho layer with the Y buffer, which itself is strained by the Nb/sapphire substrate. The subsequent tensile stress experienced by the holmium film at the interface leads to an increase in the lattice constant in the growth plane and a contraction along the growth direction (c axis). This point will be discussed in more detail later. All experiments on the film were performed at the dipole transition energy.

The data from the longitudinal and transverse scans of the magnetic peaks discussed below were fitted to various different line shapes. A Lorentzian line shape was used to fit the transverse scans obtained for the bulk sample. In the longitudinal direction, a Lorentzian squared line shape gave a slightly better fit. The transverse scans obtained for the film were fitted to a Gaussian and the longitudinal scans to a Lorentzian squared line shape. However, the specific line shapes used in the fits had only a minor influence on most of the results discussed later, and we do not consider them to be significant. In both sets of experiments transverse scans were made over large ranges, ±2° about the specular rod, both above and below the Néel temperature so that the background due to thermal diffuse scattering, Compton scattering, fluorescence, and specular reflectivity could be adequately accounted for. The background scattering was typically 10 counts per second near $L=1.75$, and varied only slightly with L between $L=1.4$ and 1.8. Throughout this work integrated intensities were obtained from both the longitudinal and transverse scans. Specifically, each scan was independently fitted as discussed above and the peak intensity and longitudinal and transverse widths were used to calculate the total integrated intensity.

V. RESULTS AND DISCUSSION

A. Order parameter and higher harmonics

Figure 1 shows the integrated intensity as a function of temperature for the $(0,0,2-\tau)$, $(0,0,2-2\tau)$, and $(0,0,2-3\tau)$ reflections (later denoted as the τ, 2τ, and 3τ peaks, respectively) of the bulk sample. The scans at the τ and 2τ peaks were taken at the maximum intensity of the dipole transition. At this energy, the peak intensity of the main magnetic satellite at $T=50$ K was a factor of about 5×10^4 weaker than that of the (0,0,2) charge scattering Bragg peak, corresponding to $\approx10^4$ counts per second. The data for the resonant third harmonic were taken at the energy of the electric quadrupole transition. As a crosscheck, we also measured the integrated intensity of the τ peak at this energy. As may be seen in Fig. 1, the ratios between the integrated intensities, I, of the peaks at $T=30$ K are $I_\tau:I_{2\tau}:I_{3\tau}=150:5:1$, in agreement with earlier experimental results,[13,14] and with calculations of the matrix elements given in Eq. (1).[40]

The integrated intensity of the principal magnetic peak at the $E1$ transition is a maximum at temperatures near 30 K (see Fig. 1), and decreases as the temperature is increased. Between 125 K and the phase transition at $T_N=131.45\pm0.05$ K, it decreases by about 2 orders of magnitude. Below 30 K, the intensity also decreases, ex-

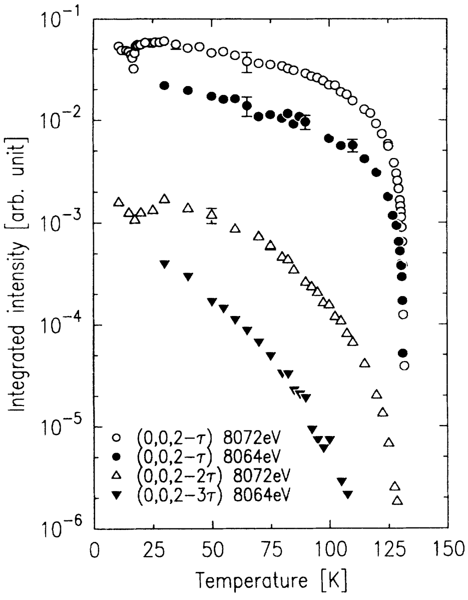

FIG. 1. Integrated intensity vs temperature for the first-, second-, and third-order resonant magnetic satellites in bulk holmium. Two of the curves are measured at the dipole transition energy (8072 eV), the other two at the quadrupole transition energy (8064 eV).

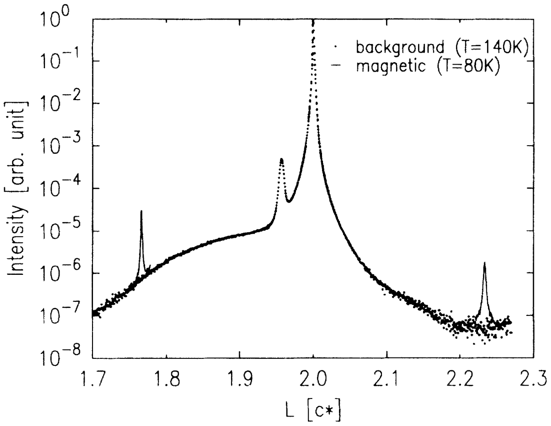

FIG. 2. Scans along the $(0,0,L)$ direction in reciprocal space at two different temperatures for the holmium film. The scan at $T=140$ K ($>T_N$) shows only the charge-scattering background with peaks at the wave vectors for the (0,0,2) reflections of the Ho and the Y layers.

hibiting a sharp minimum at the transition to the ferromagnetic cone structure, which occurred at $T_C=17$ K for cooling cycles. The behavior of the τ peak as observed at the energy of the quadrupole transition (solid circles in Fig. 1) is similar to that at the dipole transition, but is lower by a factor of about 5. The temperature dependence of the intensity of the 2τ peak is qualitatively similar to that of the τ peak. However, the intensity of the 2τ peak decreases faster with increasing temperature than that of the τ peak. Near T_C, there seems to be a drop in the intensity, similar to that which occurs for the τ peak. Unfortunately, the peak at $(0,0,2-2\tau)$ could not be detected above the background for temperatures above 127 K. The intensity of the 3τ peak is small and could be detected only for temperatures below 110 K. Its integrated intensity decreases much faster than those of the τ and 2τ peaks.

Longitudinal scans of the charge and magnetic scattering of the Ho film taken with the scattering vector along the $(0,0,L)$ direction are shown in Fig. 2. In these scans, the incident x-ray energy was tuned to the dipole maximum. The dots show the results obtained above T_N, where magnetic scattering is clearly absent. As seen in the figure, there is a broad peak centered near $L=1.9$ in addition to the (0,0,2) reflections of the Ho layer and the Y substrate (at $L=1.957$). A similar broad peak was not observed in the bulk sample. We believe that it is related to the interfacial structure of the Y/Ho/Y sandwich, and reflects the strain. For example, very simple model calculations of the scattering from a strained Ho slab show an asymmetry of the (0,0,2) Bragg peak, with increased scattering at the low L side of the peak when the layer separation (or lattice constant c) is expanded near one of the interfaces. However, detailed studies of the integrated intensity all along the specular direction for incident x-ray energies tuned near to and below the Ho L_{III} absorption edge will be required before the separate Ho and Y contributions can be identified. It is interesting in this regard that similar line shapes have also been observed at the Nb(110) reflections of Nb/sapphire interfaces by Gibaud *et al.*[46] This suggests that the broad feature observed here may ultimately originate at the sapphire interface. At 80 K, magnetic scattering is clearly visible at the $(0,0,2\pm\tau)$ reflections (solid lines, Fig. 2). Its intensity is reduced from the (0,0,2) charge scattering by $\approx 3\times 10^4$. At 30 K, the peak intensity at τ in the film was about six times smaller than observed in the bulk. However, the width of the magnetic peak in transverse scans was approximately ten times broader in the film than in the bulk sample (as will be discussed in Sec. V D). Thus, the integrated intensities in the bulk and the film are similar. Since the thickness of the Ho layer in the film (2 μm) is larger than the x-ray penetration depth (≈ 0.5 μm), the scattering volumes are comparable in the two samples.

The temperature dependence of the integrated intensities of the τ peaks of the bulk and thin-film samples are shown on a linear scale in Fig. 3. The intensities have been scaled so that they may be easily compared. At temperatures above 80 K, the variation of the integrated intensity with temperature of the film is similar to that of the bulk sample. However, the film does not show the large decrease in intensity between 15 and 20 K at the bulk transition to the ferromagnetic cone phase.

Figures 4(a) and 4(b) show the integrated intensities of the bulk magnetic scattering at τ, 2τ, and 3τ versus the reduced temperature $t=(T_N-T)/T_N$ in a double logarithmic plot. The integrated intensity, $I(n\tau)$, of the $(0,0,2-n\tau)$ peaks was fitted to a power law of the reduced temperature t with exponents x_n: $I(n\tau)\propto t^{x_n}$.

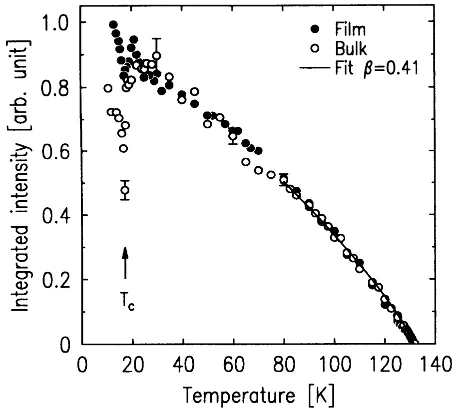

FIG. 3. Integrated intensity vs temperature for the $(0,0,2-\tau)$ magnetic satellite in bulk and film crystals of Ho. Note the dip in the intensity near the transition to the ferromagnetic phase at $T_C=17$ K in the bulk crystal. The solid line shows the fitted power-law behavior for the bulk. (The intensities of bulk and film were rescaled to agree at $T=80$ K.)

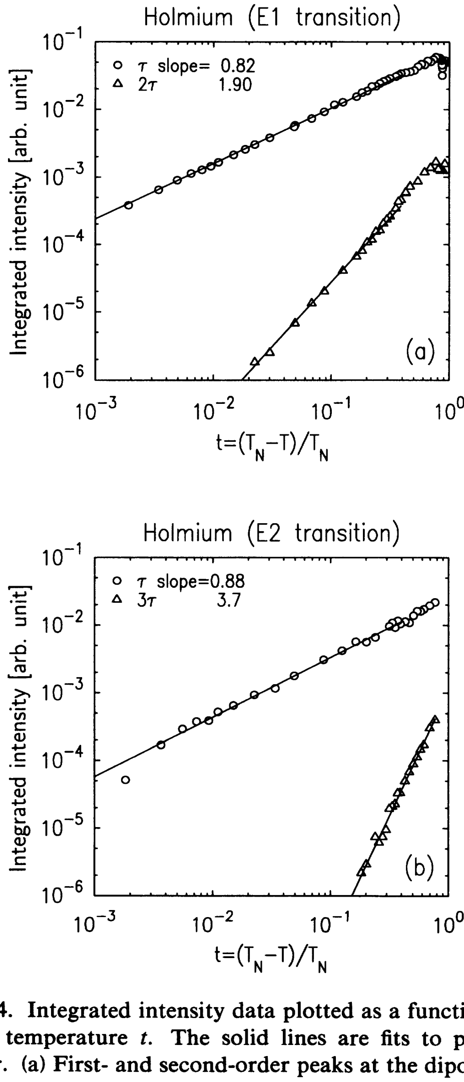

FIG. 4. Integrated intensity data plotted as a function of the reduced temperature t. The solid lines are fits to power-law behavior. (a) First- and second-order peaks at the dipole transition ($E=8072$ eV). (b) First- and third-order peaks at the quadrupole transition ($E=8064$ eV).

The value of the exponent x_n varies slightly with the temperature range used in the fits (and depends on the value of T_N used). We found that $x_1=0.82\pm0.08$ gave the overall best fit to the experimental data for temperatures above 100 K [solid line in Fig. 4(a)]. However, the fitted value of x_1 decreased slightly if the range of temperatures used in the fitting was restricted to a narrow region around T_N. Unfortunately, the number of data points close to T_N is quite limited. In the asymptotic limit of $T\rightarrow T_N$ we estimate that $x_1\rightarrow x_1'=0.78\pm0.08$. For the principal magnetic peak $x_1'=2\beta$, where β is the critical exponent for the staggered magnetization M (i.e., $M\propto t^{\beta}$). Thus, the value of the critical exponent β is found to be equal to 0.39 ± 0.04, which is in excellent agreement with the results of earlier neutron-scattering experiments.[47,48] This value is also the same within the error bars as the value $\beta=0.37\pm0.1$ reported by Thurston *et al.*[23,45,49] The value of the exponent obtained from the Ho film is $\beta=0.43\pm0.06$ ($x_1=0.86\pm0.12$). Although the average value of β is larger in the film than in the bulk, they agree to within the error bars. Both values of β agree within errors with the value predicted by Bak and Mukamel[19] on the basis of the O(4) model ($\beta=0.39$) for spiral antiferromagnets and disagree with the predictions of Kawamura's chiral model[20] ($\beta=0.25$). It should be noted that the values of T_N found for both samples fall within 1 K of each other. Since different diode thermometers were used in the two experiments, no conclusions can be made about possible differences in transition temperature between the two samples.

The fitted exponents for the temperature dependence of the integrated intensities of the 2τ and 3τ peaks are $x_2=1.9\pm0.2$ and $x_3=3.7\pm0.2$, respectively [see Figs. 4(a) and 4(b)]. Assuming mean-field scaling (i.e., $x_n=nx_1$), the exponents for the temperature dependence of the second- and third-order peaks would be expected to be $x_2=2x_1\approx1.6$ and $x_3=3x_1\approx2.5$, respectively. The measured values of the exponents are significantly larger than these values.

The principal assumption lying behind the extraction of the critical exponent β from the measured integrated intensities in these experiments is that the resonant x-ray cross section predominantly measures a two-spin correlation function, similar to that obtained in neutron diffraction. In fact, this assumption appears to be valid for both the dipolar and quadrupolar terms.[50] Specifically, Luo *et al.*[43] have recently shown that the resonant amplitude for the principal magnetic harmonic of holmium may be written as a linear combination of the orbital and spin magnetization densities, $a\mathbf{L}+b\mathbf{S}+L^2S$-products, where a and b are constants. For the heavy rare earths, where Russel-Saunders coupling is valid, this form is proportional to the magnetization provided that the higher-order terms are negligible. The magnitudes of higher-order corrections have not been calculated, but are believed to be small. It is worth noting that if the correlation functions for the dipolar and quadrupolar contributions were different, it might be expected that values of the exponent $\beta=x_1/2$ determined at the $E1$ and $E2$ resonances in Figs. 4(a) and 4(b) would also be different. While the measured values at the two energies differ slightly, $\beta(E1)=0.41\pm0.04$ and $\beta(E2)=0.44\pm0.08$, they fall comfortably within the error bars.

As discussed above, a mean-field analysis of the critical behavior predicts that the exponents x_n describing the growth of the intensity of the nth harmonic, $I(n\tau)$, should scale as n times the fundamental exponent, $x_n=nx_1$ and therefore $I(n\tau)\sim[I(\tau)]^n$. As we have seen, this scaling is not observed in holmium. In order to go beyond mean-field scaling, it is necessary to write down the order parameter for the transition and construct a Hamiltonian and a free energy. This was done for Ho in Refs. 19 and 21 using the following form for the order parameter:

$$\psi_{\pm k,P}=\sum_{\mathbf{r}} \mathbf{S}_{\mathbf{r},P}e^{\pm i\mathbf{k}\cdot\mathbf{r}} . \tag{3}$$

Here, $\mathbf{S}_{\mathbf{r},P}$ is the P component of the spin at position $\mathbf{r}$. However, further analysis of their respective Hamiltonians led these authors to quite different conclusions regarding the nature of the phase transition at T_N. At the time of writing, there is still no consensus concerning the universality class appropriate for the spiral antiferromagnets. Fortunately, there does exist a complete theory for the scaling of the higher-order harmonics in the three-dimensional XY model.[29] This theory was developed following a series of experiments on single-domain samples of freely suspended liquid crystal films.[30] Specific results for the scaling of the higher harmonic components of the bond orientational order parameter in these systems are reviewed in Appendix A. Motivated by the analysis for the XY model and by the mathematical similarity of the order parameter, Eq. (3), for the spin system in spiral antiferromagnets and the orientational order parameter in liquid crystal films, we have considered the scaling of the integrated intensity of the nth-order harmonic of the form

$$I_n=I(n\tau)=A_n[I(\tau)]^{\sigma_n} , \tag{4}$$

with the scaling exponents

$$\sigma_n=n+\lambda_n n(n-1) . \tag{5}$$

Here, λ_n is a temperature-independent parameter that may be calculated from the details of the theoretical model. As for the case of liquid crystal films, it may be assumed that λ_n depends weakly on n, and that $\lambda_n=\lambda$ may be fitted from the experimental data. A simple rewriting of Eqs. (4) and (5) shows that the deviation y from mean-field scaling, $y=\ln I_n-n\ln I_1$, is a linear function of $z=n(n-1)\ln I_1$ with slope equal to λ_n:

$$y=[\ln I_n-n\ln I_1]=\ln A_n+\lambda_n[n(n-1)\ln I_1] . \tag{6}$$

Data for the integrated intensity of the bulk sample are presented in the form suggested by Eq. (6) in Fig. 5(a). The straight lines show the best fits to this form with slopes equal to $\lambda_2=0.19$ and $\lambda_3=0.26$ for $n=2$ and 3, respectively. As may be seen in the figure, the experimental data are scattered around these best-fit lines. The uncertainty in the slopes makes it reasonable to use the same value for $\lambda_n, \lambda_n=\lambda=0.22\pm0.08$, in both cases. From Eq. (4) we find that

$$f(I_n,A_n)=[I_n/A_n]^{1/\sigma_n} \tag{7}$$

is a universal curve independent of n. This is illustrated in Fig. 5(b) which shows the scaling of the τ, 2τ, and 3τ data to the same universal curve using the value $\lambda=0.22$ to optimize the data collapse.

The assumption of temperature independence of λ_n was checked by calculating σ_2 and σ_3 at each temperature. Except at low temperatures, $T<75$ K, they were found to be approximately temperature independent. Using $\lambda=0.22$ and $x_1=0.82$, we find that the calculated values of the exponents $x_n, x_n^{\mathrm{calc}}=\sigma_n x_1$, are $x_2^{\mathrm{calc}}=2.00$ and $x_3^{\mathrm{calc}}=3.54$ for the second- and third-order satellites, respectively. This is well within the error bars of the values found by directly fitting the temperature dependence of the integrated intensities and shows that the temperature dependence of all the harmonics may be de-

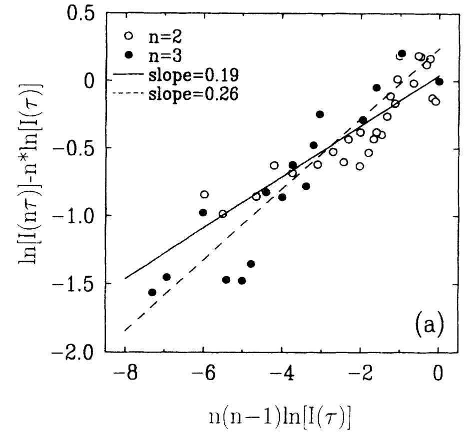

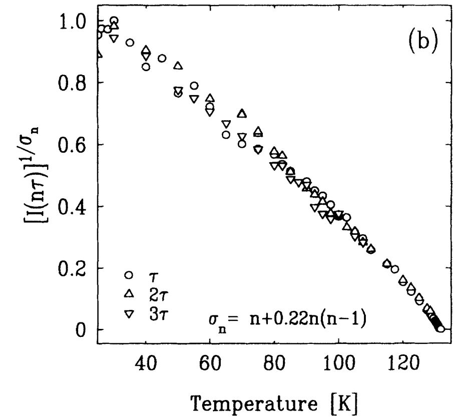

FIG. 5. (a) Deviation from mean-field scaling of the intensity of the second and third harmonics plotted vs the intensity of the primary magnetic satellite as discussed in the text. The solid and dashed straight lines are best fits to the data for $n=2$ and 3, respectively. (The highest temperatures are to the left in this figure.) (b) The rescaled, integrated intensity as a function of temperature for the magnetic satellites. The value $\lambda=0.22$ was used to obtain the best scaling to a universal curve.

scribed by only two numbers, the first exponent x_1 and the scaling parameter λ.

There are a number of obvious qualifications to this analysis. First, the assumption that Eqs. (4) and (5) may be applied to spiral antiferromagnets remains unproved. Second, the small number of harmonics observed and the limited data in the transition region prevent strong statements from being made. Third, the 2τ and 3τ peaks are not simple structural harmonics originating from higher Fourier components of the magnetic structure. Rather, they are resonant harmonics which depend on the allowed atomic electric multipole transitions, and whose detailed forms have not been fully explored (see Refs. 42–44). Nevertheless, we believe that these scaling results are interesting and hope that they may provide motivation for more work on this problem. It is possible, furthermore, that with this type of analysis a number of crossover exponents could be measured. This, in turn, would greatly facilitate the determination of the universality class of the spiral antiferromagnets.

B. Magnetic wave vector

The modulation wave vector τ, corrected for the temperature variation in the c-axis lattice constant, is plotted as a function of temperature for the film and bulk samples in Fig. 6. Close to T_N, $\tau=0.28$ for both samples, which corresponds to an average turn angle $\varphi=\tau\times 180°=50.4°$ between moments in neighboring planes along the c axis. As the temperature is reduced, τ decreases continuously. There is a clear curvature in the temperature dependence of both wave vectors, although it is more pronounced in the bulk. Joining the wave vectors at 25 K to those at 130 K by straight lines, it is seen that the maximum deviations from a linear behavior occur near 65 K in each case. Near $T_C=17.0$ K, the bulk sample exhibits a lock-in transition to $\tau=\frac{1}{6}$, which corresponds to the spiral-to-conical phase transformation. The latter is marked by an abrupt change in wave vector from $\tau=0.1795\pm0.0010$ at 17.5 K to $\tau=0.1677\pm0.0010\approx\frac{1}{6}$ at 17 K. In the diffraction pattern of the bulk, there is, in addition, a clear asymmetry in the tails of the magnetic scattering toward smaller τ about 1 K above the transition and toward larger τ within about 1 K below the transition. This asymmetry probably reflects the coexistence in bulk Ho among domains with slightly different wave vectors near $\frac{1}{6}$. In contrast, the magnetic wave vector in the film does not show a lock-in transformation to $\tau=\frac{1}{6}$. Instead, the wave vector appears to lock to the value $\tau=0.188\pm0.001$ at 10 K.

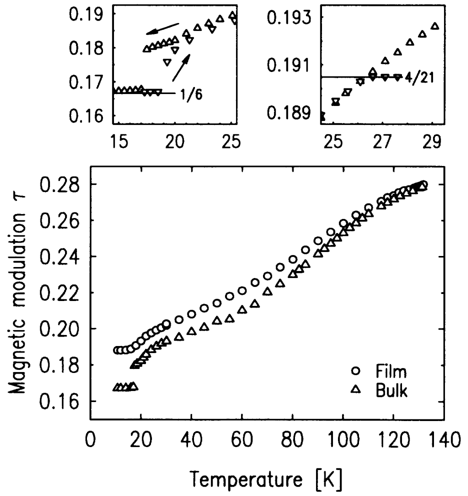

FIG. 6. The magnetic modulation wave vector τ (in c^* units) vs temperature for the bulk and film samples. The insets show the hysteresis measured near the spiral-to-conical transition of the bulk sample (left) and a lock-in transformation which was observed in the bulk sample after the temperature was cycled in a loop around $T=27$ K (right).

When the temperature of the bulk sample is raised from 10 K, the conical-to-spiral transition occurs at a higher temperature ($T_C'=19$ K) than for cooling cycles. This hysteresis in τ is shown inset in Fig. 6. A lock-in transition to $\tau=\frac{4}{21}$ was observed in the present experiments in a separate cycling of the temperature in a loop around 27 K. This is illustrated in the second inset of Fig. 6.

Qualitatively, the temperature dependence of the magnetic wave vector τ shown in Fig. 6 is similar to that observed in other holmium samples studied by x-ray and neutron diffraction.[6–12,15,51] In most studies, including those of Ho multilayers, the wave vector at T_N is observed near $\tau=0.28$, as in the present experiments. Since the magnetoelastic contributions to the free energy, which are important in determining the magnetic structure and phase behavior below T_N, are vanishingly small near T_N, the value of the magnetic wave vector at T_N is mainly determined by the position in momentum space of the maximum of the exchange energy. In some samples there has been reported a more pronounced sequence of lock-in transformations to simply commensurate wave vectors than is shown in Fig. 6 (see Refs. 8–12 and 51 and Appendix B). These latter variations among samples are well known and believed to be related to immediate sample history and to the strain present during sample growth.

There are two main differences in comparing the behavior of the wave vector of the film to that of the bulk. Both have been reported in earlier studies of various Ho thin films and multilayers.[3,6,7,51] First, the wave vectors observed in the film are (except at T_N) generally larger than observed in the bulk. Second, it is clear that the magnetic wave vector in the film does not lock to $\frac{1}{6}$. Instead, a considerably broadened magnetic peak is observed at $\tau=0.188$. It is interesting that the wave vector $\tau=0.188$ corresponds to the "supercommensurate" wave vector $\tau=\frac{3}{16}$ identified by Bates *et al.*[33] on the basis of anomalies in ultrasound measurements. In a thinner Ho film (5000 Å) studied by neutron diffraction, Jehan *et al.*[6] reported the wave vector $\tau=0.195$ at 10 K. By scanning the fifth harmonic, Jehan *et al.* further resolved their magnetic peak into the components $\tau=\frac{4}{21}=0.1905$ and $\tau=\frac{1}{5}=0.20$, and suggested coexistence among these two simply commensurate phases. These same wave vectors were also resolved in earlier scans of the fifth harmonic by neutron diffraction at 10 K of a Ho film grown simultaneously with the present film on the same sapphire substrate.[51] It appears, therefore, that x-ray- and neutron-diffraction studies of presumably equivalent 2-μm-thick films give different wave vectors at 10 K. It is possible that some of the differences observed among the films may ultimately depend on the subtleties of sample mounting, which were different in the various experiments, and also on the detailed thermal history of the samples. At present, the origin of these differences is not understood.

C. *c* axis lattice constant

The temperature dependence of the *c*-axis lattice constants below T_N, calculated from the positions of the (0,0,2) and (0,0,4) reflections, is shown in Fig. 7. Between 131 and 10 K, the *c*-axis lattice constant for the bulk sample increases by 0.66% due to magnetostriction. There is a change in slope near about 65 K and an abrupt change in magnitude near $T_C = 17$ K, at the transition to the conical phase. Hysteresis in the lattice constant between cooling and heating cycles near T_C was also observed, as illustrated in the inset of Fig. 7. The curve shown in Fig. 7 is in good agreement with earlier measurements of the thermal expansion along the *c* axis in bulk holmium[17] and with neutron-scattering studies.[52] The thermal expansion measurements[17] also showed a corresponding change in the *a*-axis lattice constant of about one-half the magnitude and of opposite sign to that observed for the *c*-axis lattice constant.

The variation with temperature of the *c*-axis lattice constant for the film is qualitatively similar to that of the bulk. However, the overall change between T_N and 25 K is only about $\frac{2}{3}$ that of the bulk. In addition, the abrupt change observed at T_C in the bulk is absent in the film, consistent with the absence of a lock-in transformation to $\tau = \frac{1}{6}$. It is interesting that the values of the *c*-axis lattice constants in the bulk and film are nearly equal only at T_N, where the magnetoelastic coupling approaches zero. Thus, there is no additional *c*-axis strain in the film relative to the bulk at T_N, although there presumably are excess in-plane strains. For temperatures decreasing from T_N, the relative differences in the *c*-axis lattice constants and wave vectors increase. In the film, the relaxation of the lattice spacing is constrained by the substrate with a larger ($\approx 2\%$) in-plane lattice constant. Presumably, this renormalizes the elastic and magnetoelastic coupling constants in the free energy, and leads to a modification of the phase behavior, including the suppression of the $\tau = \frac{1}{6}$ phase.

D. Magnetic correlation length

The temperature dependence of the longitudinal and transverse widths of the magnetic scattering measured at the $(0,0,2-\tau)$ reflection between T_N and 10 K is shown by the triangles and circles in Figs. 8 and 9 for the bulk and the film samples, respectively. The temperature dependence of the corresponding widths of the charge scattering at the (0,0,2) reflection is shown by the dashed lines. Note that the instrumental resolution has not been deconvolved from these data so that the magnetic and lattice correlation lengths cannot be read directly from the figures. In order to extract the correlation lengths, the instrumental resolution was first calculated using the procedures described by Cowley[53] and Pynn *et al.*[54] This calculation is based on the assumption that the resolution volume is controlled by the Darwin widths of the Ge(111) monochromator and analyzer crystals (0.007°) and by the divergence of the incident beam (0.014°).[55] The calculated instrumental resolution is shown as dash-dotted lines in Figs. 8 and 9. A Lorentzian line shape was then convolved in three dimensions with a Lorentzian-squared resolution function, using a triangular line shape for the out-of-plane resolution.[45] The correlation lengths were calculated as the inverse of the deconvolved half-widths.

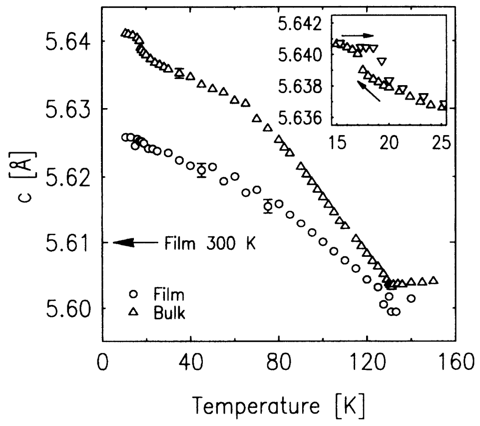

FIG. 7. The *c*-axis lattice constant vs temperature for the bulk and film samples. The inset shows the hysteresis in *c* near $T_C = 17$ K in the bulk crystal. The up and down triangles in the inset are data obtained on cooling and heating, respectively.

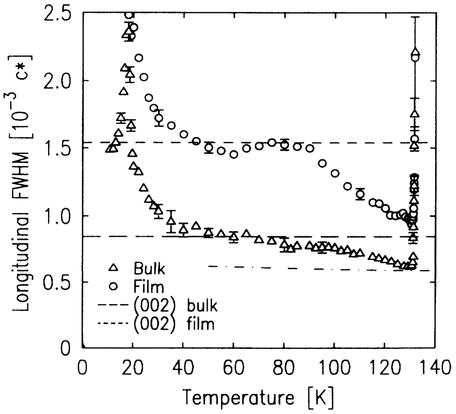

FIG. 8. Full width at half maximum of the $(0,0,2-\tau)$ magnetic satellite vs temperature for scans along the *L* direction in reciprocal space (longitudinal scans). The long- and short-dashed lines show the width of the (0,0,2) Bragg peaks for the same samples. The calculated FWHM of the instrumental resolution as discussed in the text is shown as a dash-dotted line.

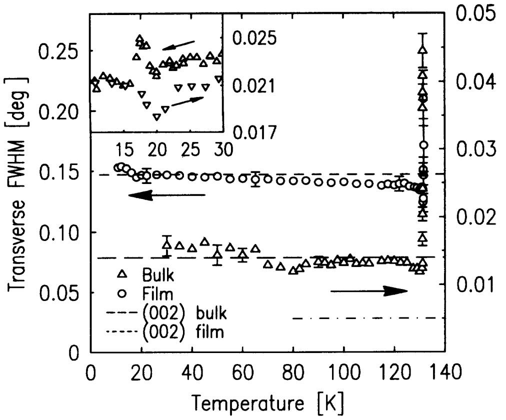

FIG. 9. Temperature dependence of the full widths at half maximum measured in transverse scans (θ scans) of the $(0,0,2-\tau)$ satellite. Dashed lines indicate the widths measured for the (0,0,2) Bragg peaks. The calculated FWHM of the instrumental resolution is shown as a dash-dotted line. The y axis for the film data is on the left side of the plot and the y axis for the bulk data is to the right. (1° FWHM corresponds to 0.034 Å^{-1} at $L=1.75$.) The inset shows data for the bulk sample at low temperatures measured in a separate experiment from those in the main figure (up/down triangles in the inset correspond to cooling/heating, respectively).

It is important to note that if the measured width of the scattering approaches the resolution width, as occurs in the present experiments for the bulk magnetic peak near T_N, then there is a large uncertainty in the resulting correlation length. For this reason, we are unable to draw firm conclusions regarding the possible presence of true long-range magnetic order in our discussion below of the bulk magnetic correlation lengths near T_N. It should also be noted that no correction has been made for the possibility of extinction in the calculation of the bulk lattice correlation lengths. The value given below must therefore be regarded as a minimum.

Referring now to Fig. 8, it may be seen that the longitudinal widths of the charge scattering (0,0,2) peak are temperature independent below 140 K, and equal to their values at room temperature. The FWHM of the instrumental resolution in the longitudinal direction is about 30% larger at the position of the (0,0,2) peak relative to that at the $(0,0,2-\tau)$ position (shown by the dash-dotted line in Fig. 8). Therefore, the longitudinal widths at (0,0,2) are nearly resolution limited in the bulk sample, corresponding to longitudinal correlation lengths of the lattice exceeding 5000 Å (which approximately equal the x-ray penetration depth). Despite the high quality of the film, which is typical of the best MBE-grown rare-earth samples, its lattice correlation length is significantly smaller than that of the bulk, namely, about 2500 Å. Similarly, the transverse widths of the charge scattering (shown by the dashed lines in Fig. 9) of the bulk and film are temperature independent, with the width found in the film ten times greater than that of the bulk. The corresponding in-plane correlation lengths are about 7000 Å in the bulk and about 500 Å in the film. The reduced translational coherence within the growth plane and along the growth axis of the film relative to the bulk reflects the increased strain in the film, and originates from the mismatch of the holmium lattice with the underlying substrate.

It is immediately clear from Figs. 8 and 9 that the longitudinal and transverse widths of the magnetic scattering from both samples increase rapidly in the critical regime as the temperature is raised above T_N. At the same time, the measured intensities decrease, and cannot be distinguished from the background at temperatures more than about 1 K above T_N. Qualitatively, this behavior is consistent with what is expected for the critical fluctuations near a second-order phase transition. However, as mentioned in the Introduction and discussed in detail in Refs. 23 and 45, the magnetic scattering in bulk holmium exhibits two length scales above T_N, one an order of magnitude longer than the other. In addition, the temperature dependence of the longer correlation length can be described as a power law with exponent $\nu \approx 1$, which is nearly twice that observed for the shorter correlation length. X-ray diffraction is especially sensitive to the longer length scale by virtue of the high resolution and the shallow penetration depth. Thus, we believe the data shown above T_N in Figs. 8 and 9 corresponds to the scattering from the sharp component, and is related to the longer length scale for both the film and bulk samples. In the bulk, the sharp component is thought to arise from a random strain distribution within the first several microns of the sample surface, which is associated with the creation of localized defects during surface preparation.[23-26,45] A similar interpretation seems straightforward in the case of the film, for which the longitudinal and transverse correlation lengths of the lattice are both shorter than the bulk, consistent with increased strain. Extensive x-ray- and neutron-scattering studies of the critical magnetic fluctuations near T_N are currently being performed on this and thinner holmium films, specifically in the hope of clarifying these issues.

The longitudinal widths of the magnetic peaks shown in Fig. 8 are also temperature dependent below T_N. The bulk magnetic width is narrowest (approaching the calculated resolution) at T_N, and increases slowly with decreasing temperature. Since the longitudinal resolution of the instrument has a broad minimum in this neighborhood of reciprocal space, this increase cannot result from the Q dependence of the resolution and signals the loss of long-range magnetic order below T_N. Near T_N, magnetic order extends over length scales at least exceeding the x-ray penetration depth (>0.5 μm). Below 30 K, there is a large increase in width to a maximum value of $2.5\times10^{-3}c^*$ at 17.5 K, which corresponds to a magnetic correlation length of only about 1100 Å along the c axis. This latter behavior is mirrored in the temperature dependence of the integrated intensity, which reaches a minimum near 17 K (Fig. 3), and in the broad distribution of spin-slip wave vectors observed above the transition to the $\frac{1}{6}$ phase. At the lock-in of the wave vector to $\frac{1}{6}$, the spin-slip density decreases abruptly to zero, and the longitudinal widths decrease (see Appendix B). Although we did not observe a variation of the widths of the charge scattering peaks with the current resolution, there are relatively large changes of the c-axis lattice constant, as has been discussed for Fig. 7. When the sample is heated from 10 K, the longitudinal width of the magnetic peak of the bulk sample remains approximately constant in the temperature range 10–20 K (data not shown). No clear broadening of the width was observed near the transition at $T'_C = 19.5$ K.

The temperature dependence of the longitudinal widths of the magnetic scattering below T_N is even more pronounced for the film, as shown by the open circles in Fig. 8. Once again, the longitudinal widths are smallest just below T_N, and increase for decreasing temperatures. Somewhat surprisingly, the longitudinal widths of the charge scattering at the (0,0,2) reflection are 60% larger than the widths of the magnetic scattering at T_N. This implies that the extent of long-range magnetic order in the film (≈ 5000 Å) exceeds the extent of c-axis translational order of the lattice (≈ 2500 Å) near T_N. As the temperature is lowered, the magnetic widths increase further. There is a shallow minimum near 60 K (where the bulk lattice constant changes slope and the magnetic wave vector approaches $\frac{2}{9}$), which is followed by a steady increase at all lower temperatures. At 10 K, the longitudinal width of the film equals $3.7\times10^{-3}c^*$, corresponding to a correlation length of only about 600 Å. Thus, the magnetic structure of the film exists in a domain state at all temperatures in the ordered phase.

The temperature dependence of the transverse widths of the charge and magnetic scattering is shown for the bulk and film samples in Fig. 9. Near and above T_N, the widths for both samples increase rapidly, consistent with the appearance of critical fluctuations, as discussed above. Below T_N, the widths are almost constant showing little variation with temperature. There is a small increase evident in the width of the bulk peak below 17 K, and observable hysteresis for temperatures increasing from 10 K, as shown in the inset of Fig. 9. The transverse correlation lengths in the film are of order 5–600 Å for both the charge and magnetic peaks within the growth plane. The corresponding correlation lengths in the bulk exceed 6000 Å.

The main contributions to the observed increase of the longitudinal widths of the magnetic peaks with decreasing temperature are likely related to the presence of competing magnetic interactions in the rare-earth metals. In particular, the rapid increase of the longitudinal magnetic widths near and below 25 K is most simply correlated with the approach of the spiral-to-conical phase transformation of the magnetic structure. In mean-field theory,[1,56] the magnetic phase behavior of holmium has been described as the result of the competition among the exchange energy $J(Q)$, the crystal-field energy and the magnetoelastic energies. As the temperature decreases, the maximum of $J(Q)$ shifts to lower wave vector and the crystal field increasingly favors alignment of the moments along the c axis. The dipolar component of the anisotropic exchange energy, which favors ferromagnetic alignment of the moments along the c axis, then shifts the maximum of $J(Q)$ toward $Q=0$. The rapidly increasing width of the magnetic peak near 25 K presumably reflects the small differences in free energy of magnetic domains with slightly different wave vectors. More generally, it has been shown by Bak and von Boehm[57] that in an Ising model with competing ferromagnetic and antiferromagnetic interactions, both commensurate and incommensurate states with long ranged magnetic order can occur, together with disordered or "discommensurate" states, depending on the relative magnitudes of the competing exchange energies. It is interesting that a similar broadening of the magnetic scattering prior to a transition from an incommensurate, antiferromagnetic state to a commensurate ferrimagnetic state has been reported in thulium by Bohr *et al.*[32]

The failure of the magnetic wave vector of the film to lock to $\tau=\frac{1}{6}$ above 10 K, together with the continuously increasing longitudinal widths below 25 K and the absence of hysteresis, imply that the film does not undergo a spiral-to-conical transition. This is not surprising in view of the suppression of the conical and ferromagnetic transitions observed for thin erbium films[58] and Dy-Y multilayers.[59] In the erbium films, for example, it has been shown that the stretching of the erbium a-axis lattice constant by the underlying Y substrate leads to a compression of the c-axis lattice constant at room temperature. The resulting modification of the two-ion magnetoelastic constants is evidently sufficient to suppress the low-temperature conical transformation in erbium. As the Y a-axis lattice constant at room temperature is 2% larger than that of holmium we might also expect a similar compression of the c-axis lattice constant relative to the bulk, and a corresponding renormalization of the phase behavior. Similar results and conclusions were reached in the study of holmium films by Jehan *et al.* and Swaddling *et al.*[6,7]

We turn now to a discussion of the fascinating differences in the lattice and magnetic correlation lengths observed just below T_N in both samples, but most clearly observed in the film (Fig. 8). It is usually the case in rare earth films that the degree of crystalline order is limited by the lattice mismatch encountered at the substrate interfaces. The interfacial structure can be complex, resulting in significant strain and concentration gradients typically thought to extend about 3–10 lattice constants along the c axis.[3,60] The increased strain in the present case is reflected by the relatively large transverse and longitudinal widths of the charge and magnetic scattering of the film in comparison to the bulk, and perhaps also by the diffuse scattering observed beneath the (0,0,2) reflection of the film shown in Fig. 2. Specifically, the (0,0,2) Bragg peak of the film is about 75% broader in the longitudinal direction than that of the bulk. This suggests that there is a significant distribution of intraplanar lattice spacings along the c axis of the film. More surprising, we have found in the film that the magnetic correlation lengths exceed the lattice correlation lengths near T_N. Similar behavior is suggested for the bulk, but the complications concerning the resolution function prevent firm conclusions. To understand this result, we note that since the intraplanar exchange interaction depends on the lattice spacing, it is plausible that the magnetic turn angle per plane may vary with the spacing to preserve the average turn angle per unit length. This variation across the film would allow the preservation of the phase of the spin-density wave, despite the limited lattice correlation length, and is reminiscent of the preservation of the magnetic wave vector across the nonmagnetic Y layers, for example, in Ho-Y multilayers.[3] It is also possible that the lattice correlation lengths are limited by in-plane defects, such as stacking faults. These would presumably have a small effect on the spiral magnetic structure, which consists of ferromagnetic sheets confined to the basal planes by the crystal field, and so would not affect the magnetic correlation length.

Finally, we comment on the loss of magnetic order for decreasing temperatures near T_N. As noted above, the crystal-field and magnetoelastic terms, which favor commensurability, compete with the exchange energy, which favors incommensurability. It is striking in this regard that the average values of the c-axis lattice constants and the magnetic wave vectors of the film and bulk samples are nearly equal just below T_N, where the extent of the magnetic order is largest and the influence of the magnetoelastic terms in the free energy is smallest. These terms are linear in the strain and increase with increasing staggered magnetization. This competition alone may be sufficient to explain the decrease of the magnetic correlation lengths when the temperature is decreased below T_N. However, this argument is usually applied under the assumption of a perfectly ordered lattice. In the present experiments, at least for the film, the crystal lattice is relatively disordered, with lattice translational correlation length smaller than the magnetic correlation length. It seems likely, therefore, that the temperature-dependent magnetoelastic strains are randomly distributed within the magnetic domains. To our knowledge, there are no detailed predictions for the magnetic phase behavior of a system with competing interactions in the presence of a random strain field. This scenario is different from that of the usual random field problem in that in the present case, the strain couples quadratically to the order parameter, not linearly.[45,61] Random strain distributions might also be expected near the surfaces of bulk crystals, where the damage from mechanical and chemical polishing is greatest. If correct, then similar broadening might be expected in the bulk, as our data suggests. It is interesting to speculate that this same interfacial strain distribution might be the origin of the second length scale observed in the critical magnetic scattering above T_N. More systematic studies of samples with controlled defect densities will be required before this question can be reasonably answered.

VI. CONCLUSIONS

Detailed, resonant x-ray scattering studies have been made of the magnetic structure and phase behavior of bulk and thin-film holmium single crystals between 10 and 300 K. The integrated intensities of the primary magnetic satellites at $(0,0,2-\tau)$ in both samples were found to exhibit power-law behavior below T_N. The measured exponents were $\beta=0.39\pm0.04$ in the bulk and $\beta=0.43\pm0.06$ in the thin film, respectively. The temperature dependence of the second- and third-order resonant satellites in the bulk also showed power-law behavior when plotted versus reduced temperature, but the values of their exponents violate simple scaling predictions of mean-field theory. We have shown that a one-parameter correction to mean-field scaling is capable of bringing the intensities of all the magnetic satellites onto a universal function of the temperature.

Systematic differences were found in the temperature dependence of the c-axis lattice constants, magnetic wave vectors, and magnetic correlation lengths of the bulk and film samples. We believe these differences originate in the strain distributions present in the two samples. In the film, the magnetic correlation length near T_N exceeds the translational correlation length of the lattice. The spiral magnetic structure forms a domain state at all temperatures in the ordered phase and shows no clear evidence of a ferromagnetic transition at low temperatures. In the bulk, longer magnetic correlation lengths were observed near T_N, but at lower temperatures the magnetic structure again forms a domain state (at least within distances of several microns from the surface). More systematic studies by x-ray and neutron diffraction on other bulk and film rare-earth samples are necessary to understand the observed behavior of the magnetic correlations. This work is in progress.

ACKNOWLEDGMENTS

We have benefited from discussions with J. D. Axe, P. Bak, L. Berman, M. Blume, J. Bohr, J. Borchers, J. Brock, P. Carra, C. P. Flynn, P. Gehring, J. P. Hannon, A. R. MacIntosh, C. Majkrzak, D. F. McMorrow, D. B. McWhan, S. G. J. Mochrie, M. Paczuski, P. Simpson, and G. Trammell. The work at Brookhaven was supported by the Division of Materials Sciences, U.S. Department of Energy under Contract No. DE AC02 76CH00016. G.H. would like to acknowledge the Research Council of Norway for financial support.

APPENDIX A: CORRECTIONS TO MEAN-FIELD SCALING IN LIQUID CRYSTAL FILMS

In x-ray experiments on freely suspended liquid crystal films Brock *et al.*[30] studied the transition from a fluid, tilted smectic phase, S_C, into a hexatic, bond orientationally ordered phase, S_I. This transition is believed to be described by a three-dimensional XY model in the presence of a small ordering field. In the liquid crystal 8OSI which was studied in Ref. 30, the bond orientational order evolves continuously on cooling from the S_C phase. Analyzing the bond orientational order as a Fourier sum of $6n$-fold symmetric terms, nine harmonics of the fundamental order parameter, C_6, were observed. These harmonics, $\{C_{6n}\}$, represent independent order parameters for the amount of $6n$-fold order present.

The order parameter in this XY system could be written as $\Psi_6=x+iy$. With $C_{6n}=\langle \mathrm{Re}(\Psi_6^n)\rangle$, each harmonic has a different symmetry and belongs to a different universality class: $C_6=\langle x\rangle$, $C_{12}=\langle (x^2-y^2)\rangle$, etc. The critical behavior of each can thus be related to the primary via a crossover exponent, ϕ_n. If a new field g_n, which couples to the nth order parameter, is introduced in the free energy, then close to the XY fixed point the free energy should scale as $F(t,g_n)=|t|^{2-\alpha}f(g_n/|t|^{\phi_n})$. Thus,

$$C_{6n} \sim |t|^{2-\alpha-\phi_n} \sim C_6^{\sigma_n} \ . \tag{A1}$$

Aharony *et al.*[29] showed that close to the XY fixed point,

$$\sigma_n = n + \lambda_n n(n-1) \ . \tag{A2}$$

The factor $n(n-1)$ comes from the number of ways the new field, g_n, can be combined with u_4, the amplitude of the fourth-order term in the Ginzburg-Landau Hamiltonian. It is believed to be general and is also present far from the transition. λ_n was calculated in Ref. 29 to be $\lambda_n = 0.3 - 0.008n$, which is only weakly dependent on n. Excellent fits to the liquid crystal data were obtained with $\lambda_n = 0.295$. λ_n was found to be essentially temperature independent until close to the transition, where there were indications of crossover to tricritical mean-field behavior. Mean-field behavior, $\sigma_n = n$, is recovered for $\lambda_n = 0$. A second limit for λ_n was obtained by Paczuski and Kardar[62] who found that $\lambda_n = 1$ in two dimensions, i.e., $\sigma_n = n^2$.

APPENDIX B: SPIN-SLIP STRUCTURES

This appendix gives a slightly more detailed discussion of the spin-slip model in holmium, and collects anecdotal descriptions of the role of sample preparation in modifying the observed magnetic structures. The first lock-in transformation in holmium (to $\tau = \frac{1}{6}$) was discovered by Koehler *et al.* in the 1960s.[8] On the basis of their observation of fifth and seventh harmonics of equal intensity in the $\tau = \frac{1}{6}$ phase, they deduced the low-temperature magnetic unit cell, describing it in terms of six "bunched" pairs of spins (doublets) oriented along the six easy directions in the basal plane. The subsequent observation of other lock-in transformations in holmium and of additional charge scattering, corresponding to lattice modulations,[11,12] has subsequently led to a description of the magnetic structure involving spin doublets and spin discommensurations, or spin slips. Spin slips occur whenever the moments of only a single atomic plane are associated with an easy direction, in contrast to a doublet in which there are two. These ideas have been discussed in detail in Refs. 1, 11, 12, 15, and 33.

A simple notation to describe the symmetry of a commensurate spin-slip structure involves listing the number of doublets and spin slips in the average magnetic unit cell. For example, 122222 corresponds to the $\tau = \frac{2}{11}$ magnetic structure with one spin-slip and five doublets for every 11 atomic planes. The factors of 2 enters because the magnetic wave vectors are usually expressed in units of the hcp chemical basis, which contains two planes. In the $\tau = \frac{5}{27}$ phase there are four doublets and one spin-slip for every nine atomic planes (12222 12222 12222 12222 12222 12222). The wave vector is computed by noting that there are five full 2π rotations of the moments for every 54 atomic planes: $\tau = (\frac{5}{54} \times 2)$.[12]

Simply commensurate spin-slip structures are those in which the ratio of doublets to spin slips is an integer, e.g., $\frac{2}{9}$ (12 12 12), $\frac{1}{5}$ (122 122), $\frac{4}{21}$ (1222 1222 1222), $\frac{5}{27}$, $\frac{2}{11}$, and $\frac{1}{6}$. Lock-in transformations to simply commensurate wave vectors have been observed in a number of samples.[6–12,15,51] Higher-order commensurate phases are those in which the ratio of doublets to spin slips is a rational number, e.g., $\tau = \frac{1}{4}$ (112 112). As may be seen, in this case the spacing between spin slips is not unique. Lock-in transformations to higher-order commensurate phases have been observed in samples subjected to a magnetic field,[63,64] and in the current studies of a thin film in zero field ($\tau = \frac{3}{16} \approx 0.188$).

Incommensurate spin-slip structures may be defined as those in which the ratio of doublets and spin slips is an irrational number. However, it is not clear whether any truly incommensurate spin-slip structures have been observed in holmium. For example, at higher temperatures, when approximately resolution-limited, incommensurate magnetic peaks are observed in bulk, the relevant crystal field and magnetoelastic terms in the free energy are small, and a spin-slip description of the magnetic structure may be inappropriate.[1] What is probably more commonly observed at lower temperatures are disordered spin-slip structures in which there is a finite distribution of spin-slip spacings. In scattering experiments, disordered spin-slip structures can be identified if the longitudinal widths of their magnetic peaks are broader than the resolution. This is clearly the case at lower temperatures for both the film and the bulk in the present experiments, as shown in Fig. 8. Finally, we note that Bates *et al.*[33] have identified another class of commensurate spin-slip structures, called "supercommensurate" structures. These correspond to spin-slip structures whose symmetry breaks the hexagonal symmetry of the lattice, leading to anomalies in the temperature dependence of the elastic constants. Some examples include the $\tau = \frac{1}{4}$, $\frac{1}{5}$, $\frac{3}{16}$, and $\frac{2}{11}$ phases.

An important element of the spin-slip description of rare-earth magnetic structures involves the lattice modulations which arise from the spin-slip distribution.[11,12] In the $\tau = \frac{5}{27}$ phase, for example, there is one spin-slip for every nine atomic planes. The corresponding spin-slip wave vector is $\tau_s = \frac{2}{9}$, which locates the satellite positions at which additional charge scattering has been found in x-ray scattering experiments. The temperature dependence of the magnetic and spin-slip wave vectors, τ and τ_s, respectively, for the bulk sample studied in the present work is shown by the open and solid squares in Fig. 10. Also shown in the figure is the temperature dependence of τ and τ_s obtained from already published x-ray scattering measurements of a different bulk sample.[11,12] In each case, the magnetic and spin-slip wave vectors satisfy the simple relation $\tau_s = 12\tau - 2$.[12] Thus, when the magnetic wave vector $\tau = \frac{2}{11}$, so does the spin-slip wave vector τ_s. And, when the magnetic wave vector locks to $\tau = \frac{1}{6}$, the spin-slip wave vector approaches zero.

The first observation that the detailed temperature dependence of the magnetic wave vector of holmium can

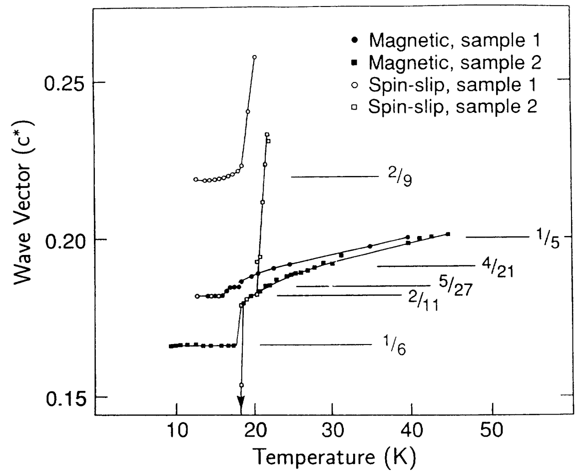

FIG. 10. Temperature dependence of the magnetic (solid symbols) and spin-slip (open symbols) wave vectors for two different bulk samples studied by x-ray diffraction. The squares are data taken for the bulk sample discussed in this paper. The circles correspond to data taken from Refs. 11 and 12. The wave vector of the spin slips broadens considerably and moves to zero when the magnetic wave vector locks to $\frac{1}{6}$, as indicated by the arrow.

vary with samples was made by Koehler *et al.*[8] In the intervening years, these variations have become well known and are usually attributed to the strain present in the sample, to the possible presence of chemical impurities, and to immediate sample history. Indeed, striking differences between the bulk and film samples studied here are given in the text. Along these lines, it is worth noting that surface preparation can also apparently alter the magnetic structure in the ordered phase within the first several microns of a sample in comparison to its bulk behavior. Here, we include the cutting and polishing procedures, both mechanical and electrochemical, which affect the surface and near-surface morphology in the term surface preparation.[11] These introduce excess strain in addition to the natural oxidation, which occurs for metals in air. An example of the affect of surface preparation on the magnetic properties was found in early x-ray magnetic scattering studies of a holmium sample for which, unfortunately, the exact surface preparation is unknown.[11,12,51] In those experiments a larger set of wave vectors was observed between 30 and 10 K by neutron diffraction than by x-ray diffraction. The temperature dependence of the magnetic wave vector observed for that sample by x-ray diffraction is reproduced in Fig. 10 (solid circles).[11,12] There are suggestions of lock-in behavior at $\tau=\frac{5}{27}$ and $\frac{2}{11}$, but no evidence for a lock-in transition to $\tau=\frac{1}{6}$. Subsequent neutron-diffraction studies of the temperature dependence of the fifth magnetic harmonic of the same sample, however, clearly showed coexistence among the wave vectors $\frac{5}{27}$, $\frac{2}{11}$, and $\frac{1}{6}$ at low temperatures. Indeed, the scattering at $\tau=\frac{1}{6}$ was dominant in the neutron-diffraction experiments.[11] Under the assumption that the near-surface properties might differ from the bulk, these differences were attributed to the smaller sample volume probed by x-ray diffraction (penetration depth $\approx 1\ \mu$m) relative to neutron diffraction (penetration depth ≈ 1 cm). For comparison, the temperature dependence of the magnetic wave vector of the current sample obtained by x-ray diffraction is also shown in the figure (solid squares). The lock-in transformation to $\tau=\frac{1}{6}$ in these data is very clear. Moreover, they agree quantitatively with the results of neutron diffraction from this sample at all temperatures below T_N.[45]

---

[*] Present address: Institutt for Energiteknikk, N-2007 Kjeller, Norway.

[1] J. Jensen and A. R. Macintosh, *Rare Earth Magnetism* (Clarendon, Oxford, 1991).

[2] For recent reviews, see W. G. Stirling and G. H. Lander, Synchr. Rad. News **5**(4), 17 (1992); D. Gibbs, *ibid.* **5**(5), 18 (1992).

[3] C. F. Majkrzak, J. Kwo, M. Hong, Y. Yafet, D. Gibbs, C. L. Chien, and J. Bohr, Adv. Phys. **40**, 99 (1991).

[4] R. S. Beach, J. A. Borchers, A. Matheny, R. W. Erwin, M. B. Salamon, B. Everitt, K. Pettit, J. J. Rhyne, and C. P. Flynn, Phys. Rev. Lett. **70**, 3502 (1993), and references therein.

[5] F. Tsui and C. P. Flynn, Phys. Rev. Lett. **71**, 1462 (1993).

[6] D. A. Jehan, D. F. McMorrow, R. A. Cowley, R. C. C. Ward, M. R. Wells, N. Hagmann, and K. N. Clausen, Phys. Rev. B **48**, 5594 (1993).

[7] P. P. Swaddling, D. F. McMorrow, J. A. Simpson, M. R. Wells, R. C. C. Ward, and K. N. Clausen, J. Phys. Condens. Matter **5**, L481 (1993).

[8] W. C. Koehler, J. W. Cable, M. K. Wilkinson, and E. O. Wollan, Phys. Rev. **151**, 414 (1966).

[9] G. P. Felcher, G. H. Lander, T. Arai, S. K. Sinha, and F. H. Spedding, Phys. Rev. B **13**, 3034 (1976).

[10] M. J. Pechan and C. Stassis, J. Appl. Phys. **55**, 1900 (1984).

[11] D. Gibbs, D. E. Moncton, K. L. D'Amico, J. Bohr, and B. H. Grier, Phys. Rev. Lett. **55**, 234 (1985).

[12] J. Bohr, D. Gibbs, D. E. Moncton, and K. L. D'Amico, Physica A **140**, 349 (1986).

[13] D. Gibbs, G. Grübel, D. R. Harshman, E. D. Isaacs, D. B. McWhan, D. Mills, and C. Vettier, Phys. Rev. Lett. **61**, 1241 (1988).

[14] D. Gibbs, G. Grübel, D. R. Harshman, E. D. Isaacs, D. B. McWhan, D. Mills, and C. Vettier, Phys. Rev. B **43**, 5663 (1991).

[15] R. A. Cowley and S. Bates, J. Phys. C **21**, 4113 (1988).

[16] J. Wang, D. P. Belanger, and B. D. Gaulin, Phys. Rev. Lett. **66**, 3195 (1991); B. D. Gaulin, M. Hagen, and H. R. Child, J. Phys. (Paris) Colloq. **49**, C8-327 (1988).

[17] D. A. Tindall, M. O. Steinitz, and M. L. Plumer, J. Phys. F **7**, L263 (1977); M. O. Steinitz, M. Kahrizi, and D. A. Tindall, Phys. Rev. B **36**, 783 (1987).

[18] A. M. Venter, P. V. du Plessis, G. A. Eloff, and E. Fawcett, J. Phys. Condens. Matter **2**, 1363 (1990).

[19] P. Bak and D. Mukamel, Phys. Rev. B **13**, 5086 (1976).

[20] H. Kawamura, J. Appl. Phys. **63**, 3086 (1988).

[21] Z. Barak and M. B. Walker, Phys. Rev. B **25**, 1969 (1982).

[22] P. Azaria, B. Delmotte, and T. Jolicouer, Phys. Rev. Lett. **64**,

3175 (1990).

[23] T. R. Thurston, G. Helgesen, D. Gibbs, J. P. Hill, B. D. Gaulin, and G. Shirane, Phys. Rev. Lett. **70**, 3151 (1993).

[24] P. Gehring, K. Hirota, C. F. Majkrzak, and G. Shirane, Phys. Rev. Lett. **71**, 1087 (1993).

[25] S. Langridge, W. G. Stirling, G. H. Lander, J. Rebizant, J. C. Spirlet, D. Gibbs, and O. Vogt, Europhys. Lett. **25**, 137 (1994).

[26] G. Watson, B. D. Gaulin, D. Gibbs, G. H. Lander, and T. R. Thurston (unpublished).

[27] T. W. Ryan, R. J. Nelmes, R. A. Cowley, and A. Gibaud, Phys. Rev. Lett. **56**, 2704 (1986).

[28] D. F. McMorrow, N. Hamaya, S. Shimomura, Y. Fujii, S. Kishimoto, and H. Iwasaki, Solid State Commun. **76**, 443 (1990), and references therein.

[29] A. Aharony, R. J. Birgeneau, J. D. Brock, and J. D. Litster, Phys. Rev. Lett. **57**, 1012 (1986).

[30] J. D. Brock, A. Aharony, R. J. Birgeneau, K. W. Evans-Lutterrodt, J. D. Litster, P. M. Horn, G. B. Stephenson, and A. R. Tajbakhsh, Phys. Rev. Lett. **57**, 98 (1986).

[31] L. Wu, M. J. Young, Y. Shao, C. W. Garland, R. J. Birgeneau, and G. Heppke, Phys. Rev. Lett. **72**, 376 (1994).

[32] J. Bohr, D. Gibbs, and K. Huang, Phys. Rev. B **42**, 4322 (1990).

[33] S. Bates, C. Patterson, G. J. McIntyre, S. B. Palmer, A. Mayer, R. A. Cowley, and R. Melville, J. Phys. C **21**, 4125 (1988).

[34] F. de Bergevin and M. Brunel, Phys. Lett. **39A**, 141 (1972).

[35] K. Namikawa, A. Ando, T. Nakajima, and H. Kawata, J. Phys. Soc. Jpn. **54**, 4099 (1985).

[36] E. D. Isaacs, D. B. McWhan, C. Peters, G. E. Ice, D. P. Siddons, J. B. Hastings, C. Vettier, and O. Vogt, Phys. Rev. Lett. **62**, 1671 (1989); D. B. McWhan, C. Vettier, E. D. Isaccs, G. E. Ice, D. P. Siddons, J. B. Hastings, C. Peters, and O.Vogt, Phys. Rev. B **42**, 6007 (1990).

[37] C. C. Tang, W. G. Stirling, G. H. Lander, D. Gibbs, W. Herzog, P. Carra, B. T. Thole, K. Mattenberger, and O. Vogt, Phys. Rev. B **46**, 5287 (1992).

[38] C. Kao, J. B. Hastings, E. D. Johnson, D. P. Siddons, G. C. Smidt, and G. A. Prinz, Phys. Rev. Lett. **65**, 373 (1990).

[39] J. M. Tonnerre, M. Jergel, D. Raoux, M. Idir, G. Soullier, R. Barchewitz, and B. Rodmacq, J. Magn. Magn. Mater. **121**, 230 (1993).

[40] J. P. Hannon, G. T. Trammel, M. Blume, and D. Gibbs, Phys. Rev. Lett. **61**, 1245 (1988).

[41] M. D. Hamrick, M. A. thesis, Rice University, Texas, 1991.

[42] P. Carra and B. T. Thole, Rev. Mod. Phys. (to be published).

[43] J. Luo, G. T. Trammel, and J. P. Hannon, Phys. Rev. Lett. **71**, 287 (1993).

[44] M. Blume, *Proceedings of the Second International Conference on Anomalous Scattering* (Elsevier, Amsterdam, 1993).

[45] T. R. Thurston, G. Helgesen, J. P. Hill, Doon Gibbs, B. D. Gaulin, and P. Simpson, Phys. Rev. B **49**, 15 730 (1994).

[46] A. Gibaud, R. A. Cowley, D. F. McMorrow, R. C. C. Ward, and M. R. Wells, Phys. Rev. B **48**, 14 463 (1993).

[47] J. Eckert and G. Shirane, Solid State Commun. **19**, 911 (1976).

[48] G. H. F. Brits and P. V. du Plessis, J. Phys. F **18**, 2659 (1988).

[49] The reason for the larger error bars in the paper of Thurston *et al.* (Ref. 23) stems from a larger uncertainty in T_N, which was estimated both from the behavior of the intensity below T_N and from fits to a two-component line shape for the critical scattering above T_N. It may also be noted that our own neutron-scattering experiments on this sample gave a somewhat lower value ($\beta=0.3$), which we interpret as being due to extinction, and which we believe is absent in the x-ray-scattering experiments.

[50] M. Blume, P. Carra, and J. P. Hannon (private communication).

[51] D. Gibbs, J. Less-Common Met. **148**, 109 (1989).

[52] F. J. Darnell, Phys. Rev. **130**, 1825 (1963).

[53] R. A. Cowley, Acta Crystallogr. A **43**, 825 (1987).

[54] R. Pynn, Y. Fujii, and G. Shirane, Acta Crystallogr. A **39**, 38 (1983).

[55] D. L. Abernathy, S. G. J. Mochrie, D. M. Zehner, G. Grübel, and D.Gibbs, Phys. Rev. B **45**, 9272 (1992).

[56] C. C. Larsen, J. Jensen, and A. R. Mackintosh, Phys. Rev. Lett. **59**, 712 (1987).

[57] P. Bak and J. von Boehm, Phys. Rev. B **21**, 5297 (1980).

[58] J. A. Borchers, M. B. Salamon, R. W. Erwin, J. J. Rhyne, R. R. Du, and C. P. Flynn, Phys. Rev. B **43**, 3123 (1991); J. A. Borchers, M. B. Salamon, R. W. Erwin, J. J. Rhyne, G. J. Nieuwenhuys, R. R. Du, C. P. Flynn, and R. S. Beach, *ibid.* **44**, 11 814 (1991).

[59] M. B. Salamon, S. Sinha, J. J. Rhyne, J. E. Cunningham, R. W. Erwin, J. A. Borchers, and C. P. Flynn, Phys. Rev. Lett. **56**, 259 (1986).

[60] R. W. Erwin, J. J. Rhyne, M. B. Salamon, J. Borchers, S. Sinha, R. Du, J. E. Cunningham, and C. P. Flynn, Phys. Rev. B **35**, 6808 (1987).

[61] J. D. Axe (private communication).

[62] M. Paczuski and M. Kardar, Phys. Rev. Lett. **60**, 861 (1988).

[63] R. A. Cowley, D. A. Jehan, D. F. McMorrow, and G. F. McIntyre, Phys. Rev. Lett. **66**, 1521 (1991).

[64] D. A. Tindall, M. O. Steinitz, and T. M. Holden, Phys. Rev. B **47**, 5463 (1993).